Classification
Physics Abstracts
07.80 — 61.46 — 82.80

Quantitative Elemental Distribution Image of a Carbon Nanotube

Hiroki Kurata, Seiji Isoda and Takashi Kobayashi

Institute for Chemical Research, Kyoto University, Uji, Kyoto 611, Japan

(Received May 10; accepted August 4, 1995)

Abstract. — Energy-filtering transmission electron microscopy was applied to carbon nanotubes in order to investigate quantitative property of elemental maps obtained by inelastically scattered electrons corresponding to the carbon K-edge. An 1 MeV high-resolution electron microscope (JEOL, ARM-1000) equipped with a GATAN imaging filter was employed. Because of a cylindrical structure of nanotubes the number of carbon atoms contributing to the image changes across the tube axis. We could detect the contrast difference due to 20 carbon atoms in the carbon distribution image of 6 layers tube. Furthermore, we examined the carbon mapping from a conical tip region with progressive closure of carbon layers, where an intensity profile clearly distinguishes the difference of 6 graphene sheets. From the consideration of signal-to-noise ratio, the detection limit is concluded to be less than 22 carbon atoms in the present experimental conditions.

1. Introduction

Energy-filtering transmission electron microscopy (EFTEM) [1] provides energy-filtered high-resolution image and diffraction pattern, and also elemental map, which promise quantitative analyses of specimens. In particular the elemental mapping by recording the core-loss signal makes it possible not only to visualize a two-dimensional distribution of a particular element, but also to count the number of atom existing in a specific region by analyzing the image intensity quantitatively. Recently Berger *et al.* [2] have demonstrated the oxygen distribution image taken from the amorphous grain boundary films in sintered Si_3N_4 ceramics using EFTEM. They emphasized that the detection limit is governed by the signal-to-noise ratio of the image, which depends on the instrumental parameters and specimens. The optimum imaging conditions for elemental mapping have been investigated theoretically by Berger and Kohl [3, 4]. It has become of interest in recent years to estimate the detection limit. In order to evaluate the detection limit experimentally under given imaging conditions, the precise thickness of specimen is needed to be known and the thickness should be thin enough to avoid multiple scattering effects because it disturbs the intensity distribution somewhat.

The structure of carbon nanotubes is characterized by the inner and outer diameters and the number of graphene sheet [5]. The typical size of a tube is the order of nanometers which is thin

enough to analyze the intensity of the elemental distribution image without any corrections on multiple scattering. Since the structural parameters of each nanotube can be determined definitely from a high-resolution electron micrograph, the carbon distribution image observed from a well-defined nanotube is very suitable for examining the quantitative property of the elemental mapping.

In the present work, we investigate the carbon distribution images observed from a single nanotube and the conical tip region of a tube. The intensity profile of the image is compared with the distribution of the number of carbon atoms estimated by a cylindrical structure model of the nanotube. The image quality is evaluated using the signal-to-noise ratio calculated from the intensity of the carbon distribution image and the background image, and the detection limit is discussed.

2. Experimental

The investigations were performed using the JEOL ARM-1000 (operated at 1 MeV) [6] equipped with the Gatan imaging filter (GIF) [7-9]. The aberration constants of the objective lens are $C_s = 1.7$ mm and $C_c = 3.6$ mm. The filtered image is recorded by a 1024 × 1024 slow-scan CCD camera with the element size of 24 × 24 μm^2. The performance of the CCD camera for 1 MeV operation has been recently investigated by Mooney *et al.* [10]. They reported the performance similar to that of the fiber-optically coupled camera running at 100 keV.

High resolution lattice image and carbon distribution image of self-supported nanotubes were observed at a magnification of the microscope of 20,000x which corresponds to an effective magnification of 340,000x on the slow-scan CCD camera of the GIF. This means that the pixel size referred back to the objective plane is 0.07 nm which allows us to observe the elastic image of the (002) lattice planes ($d = 0.34$ nm) of graphite. This magnification is, therefore, enough to characterize the structure of each nanotube by imaging graphene layers. In the carbon distribution images, however, the intensities of 4 × 4 pixels were integrated into one effective pixel (binning mode) because of the small inelastic scattering cross-section of the carbon K-edge compared to that of elastic scattering, so that the effective pixel size became 0.28 nm. The inelastic scattering images were observed with an electron dosage of 1.25×10^7 electron/nm^2. Under such strong irradiation some kinds of lattice distortion might occur, but it was not so serious because the shape transformations in nanotubes recently reported by Ajayan *et al.* [11] was not observed. The collection semi-angle β restricted by the size of the objective aperture and the width of an energy selecting slit δE of GIF were set to be 10 mrad and 30 eV, respectively. Under these conditions the chromatic broadening [12] due to the aberration of the objective lens is almost the same as the size of a binned pixel. The carbon distribution images were obtained by subtracting the background image from the post carbon K-edge image using the three windows technique [13]: two pre-edge images were taken at 239 ± 15 and 269 ± 15 eV for the background subtraction procedure. The post-carbon K-edge image was observed at 304 ± 15 eV. The exposure time of each inelastic image was 10 s.

3. Results and Discussion

Typical elastic and carbon distribution images of a single nanotube observed at low magnification are shown in Figures 1a and 1b, respectively. In the carbon image we can observe a weak contrast at the central part and the tip region of the tube. For detail analysis we observed each part at high magnification. A high-resolution lattice image and the corresponding carbon distribution image of a nanotube are shown in Figures 2a and 2b. The intensity profiles across the tube axis of these

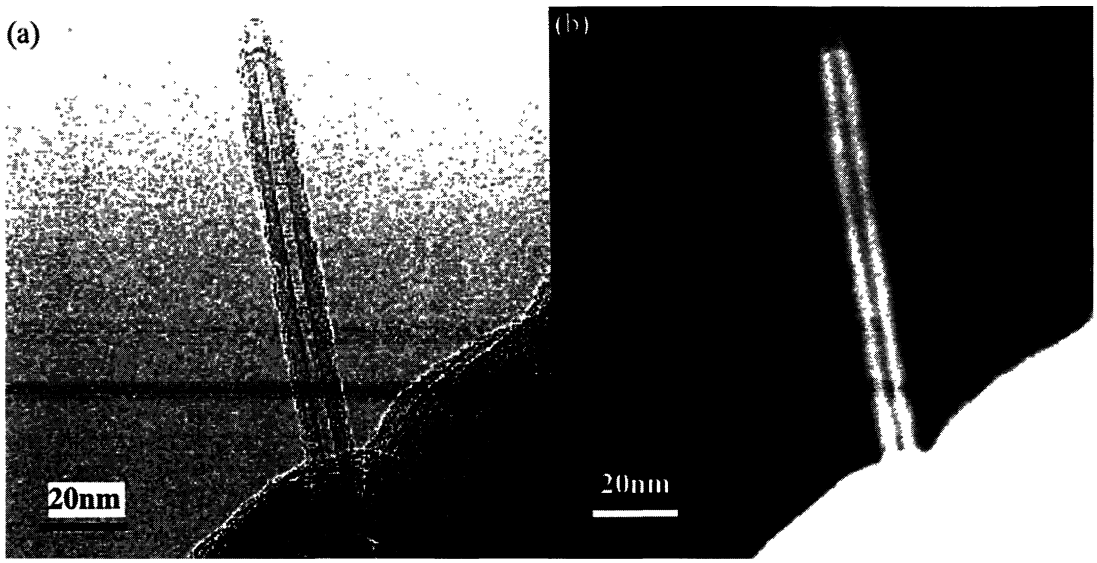

Fig. 1. — Elastic image of single nanotube a) and its carbon distribution image b).

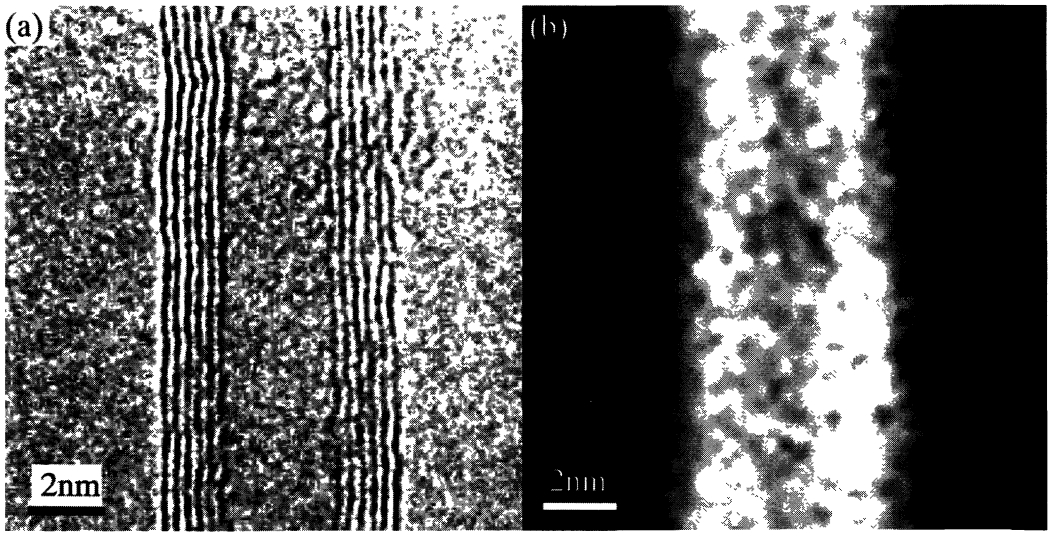

Fig. 2. — a) High-resolution lattice image of single nanotube and b) corresponding carbon distribution image.

images are shown in Figure 3. The high-resolution lattice image and its intensity profile indicate clearly the 6 layers cylindrical structure as the lattice fringes due to the (002) planes at both sides of the tube. The outer and inner diameters were measured to be 6.5 nm and 3.15 nm, respectively. Although the carbon image is a little noisy compared to one observed at low magnification, the line profile across a tube axis indicates clearly that the intensity change is proportional to the number of carbon atoms. The intensity of the carbon profile increases from the vacuum to the inside of the

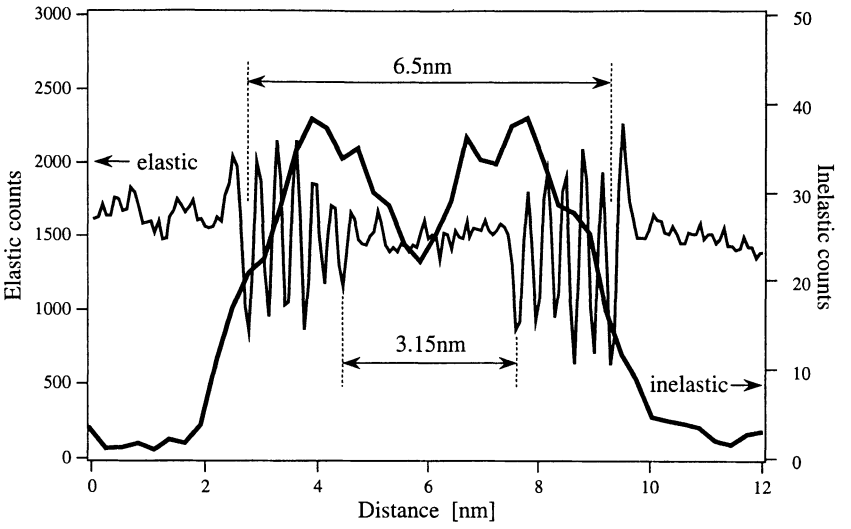

Fig. 3. — Intensity profiles across the tube axis of the lattice image and the carbon distribution image of Figure 2.

tube, which indicates the increase of the number of carbon atoms. And the decrease in the middle suggests the hollow structure of the tube. The similar variation of intensity of the carbon K-edge of the nanotube filled with manganese was reported by Ajayan *et al.* [14] using the coupling of the parallel EELS and a scanning TEM, where they distinguished clearly the distribution of both elements (C and Mn). Here we relate quantitatively such a characteristic carbon profile to the atomic distribution determined by the following procedure.

In order to calculate the intensity of carbon image, I_i, at a binned pixel i of the detector, we start from the following equation,

$$I_i(\beta, \delta E) = D \cdot \sigma(\beta, \delta E) \cdot N_i \cdot \eta. \tag{1}$$

Here D (e^-/nm^2) is the electron dosage irradiated on the specimen, $\sigma(\beta, \delta E)$ is the partial inelastic scattering cross-section of the carbon K-edge with the collection angle β of 10 mrad and the energy window δE of 30 eV. In the inelastic scattering of 1 MeV electrons, relativistic effects become significant. Following the relativistic Bethe theory [13, 15], the energy differential cross-section can be represented by

$$\frac{d\sigma}{dE} = \frac{4\pi a_0^2 R^2}{ET} \cdot \frac{df}{dE} \cdot \left[\ell n(1 + \beta^2/\theta_E^2) + 2\ell n\gamma - v^2/c^2\right] \tag{2}$$

where a_0 is the Bohr radius, $R = 13.6$ eV is the Rydberg energy, v and c are the velocity of the incident electron and light, $\gamma = (1 - v^2/c^2)^{-1/2}$ is the relativistic factor, E is the loss-energy, $T = m_0 v^2/2$ is the relativistic energy, $\theta_E = E/2\gamma T$ is the characteristic scattering angle. The last two terms in the Equation (2) arise from the relativistic retardation effect. Neglecting these terms gives the nonrelativistic cross-section which can be calculated using the SIGMAK2 software [13]. The contribution from the retardation effect is always positive and estimated to be about 17%, so that the nonrelativistic cross-section multiplied by the scale factor of 1.17 is used in the present analysis. The η in Equation (1) is the conversion efficiency of the detection system of the GIF, which was measured to be 0.3. N_i in Equation (1) is the number of carbon atom projected to the

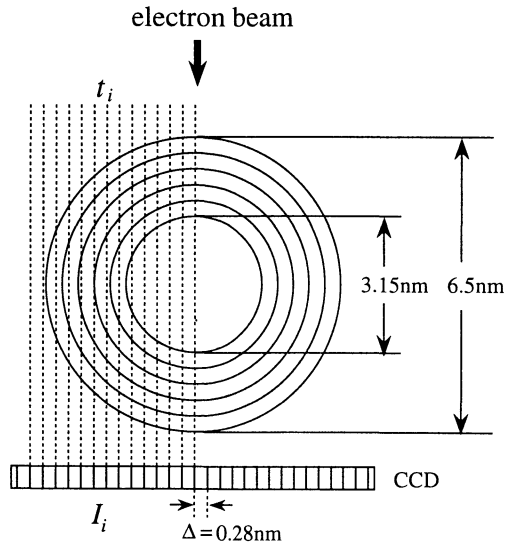

Fig. 4. — Cross-section model of the 6 layers nanotube to estimate the number of carbon atoms contributing the carbon distribution image. The effective pixel size is 0.28 nm due to the binning.

binned pixel i of the detector, which is estimated using the structure model of Figure 4, in which the cross section of the nanotube across the tube axis consists of six concentric graphene circles. The N_i can be represented by the Equation,

$$N_i = t_i \cdot \Delta \cdot \rho. \tag{3}$$

Here t_i is the sum of length of graphene arcs cut by the size of each binned pixel, Δ the pixel size (= 0.28 nm) and ρ the in-plane carbon density (= 38 atoms/nm^2) estimated from one graphite layer.

The experimental and theoretical intensity profiles are compared in Figure 5. The agreement of both profiles is quite satisfactory except for a little broadening of the experimental profile. This agreement means that the elemental distribution image is highly quantitative as long as thin specimens are examined. The slight broadening of the carbon profile is probably attributed to the delocalization effect [16, 17] of the inelastic scattering event and the chromatic broadening [12] due to the objective lens. The intensity maxima and minimum at the central region of the nanotube correspond to 55 and 35 carbon atoms per binned pixel, respectively. Therefore, we conclude that the difference of 20 carbon atoms can be discriminated at nanometer scale with a good signal-to-noise ratio. At the periphery of the tube the intensity of about 15 counts on CCD corresponds to 22 carbon atoms per pixel, which is the smallest number of atom detected by the present experiment.

Next example of carbon distribution image is the observation of the conical tip region of nanotube as shown in Figure 6. The lattice image (Fig. 6a) shows that the tip is made by progressive multilayers of curved graphene sheets. In this case the numbers of multilayers are 5, 8 and 14 layers from the tip to the inside of the tube. Since the tip has a conical symmetry about the cone axis, the number of carbon atoms projected on one pixel of the detector is expected to be constant in the respective multilayer region. Such distribution of the carbon atoms can be visualized by the elemental mapping. The carbon distribution image taken from the same region (Fig. 6b) shows

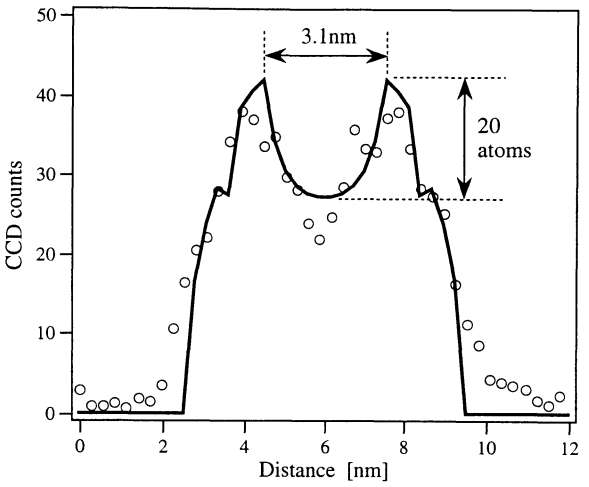

Fig. 5. — Comparison between the experimental intensity profile and the calculated one.

the stepwise intensity change from the tip to the inside of the tube as expected from the increase of graphene layers. The line profile of the image along the cone axis is shown in Figure 6c. The step like change in the intensity profile indicates the progressive increase of graphene multilayers. The differences of the step height correspond to 6 and 12 graphene layers, respectively, because the electron beam travels through the upper and lower multilayers of the nanotube. Such differences of the graphene layers are equivalent to 18 and 36 carbon atoms per binned pixel, respectively. These numbers of atoms can be calculated as follows: because the tip has a vertical angle of 20 degree, which means the multilayers inclined about 10 degree from the array of CCD elements, the number of carbon atoms in the n layers projected to one binned pixel is given

$$N(n) = 2\frac{\Delta^2}{\cos 10^\circ} \cdot n \cdot \rho. \tag{4}$$

Using this Equation, the number of carbon atoms in one binned pixel corresponding to the difference of 6 graphene layers is calculated by $N(8) - N(5)(= 6 \times 0.28^2 \times 38/\cos 10^\circ = 18)$. In this example, therefore, we can detect the difference of about 18 carbon atoms.

Finally, we discuss the statistical properties of the carbon distribution image of Figure 1b by means of the signal-to-noise ratio (SNR). The SNR is deduced from the observed images using the following Equation [2, 13],

$$\mathrm{SNR} = I_i^{\mathrm{s}} \cdot \sqrt{\frac{\mathrm{DQE}}{I_i^{\mathrm{s}} + h \cdot I_i^{\mathrm{b}}}}. \tag{5}$$

Here I_i^{s} and I_i^{b} are the number of electrons contributing to the intensity at the binned pixel i of the carbon distribution image and the background image, respectively. The background image is extrapolated using the three windows technique assuming the power-law energy dependence of background intensity. h is the parameter to specify the quality of the background subtraction procedure and depends on the positions of the three windows to take the pre- and post-carbon K-edge images [4]. In the present experiment h was 7. The detection quantum efficiency of the detector system, DQE, was assumed to be 0.7. In general cases, the noise component coming from the background extrapolation procedure determines the SNR dominantly. In the present

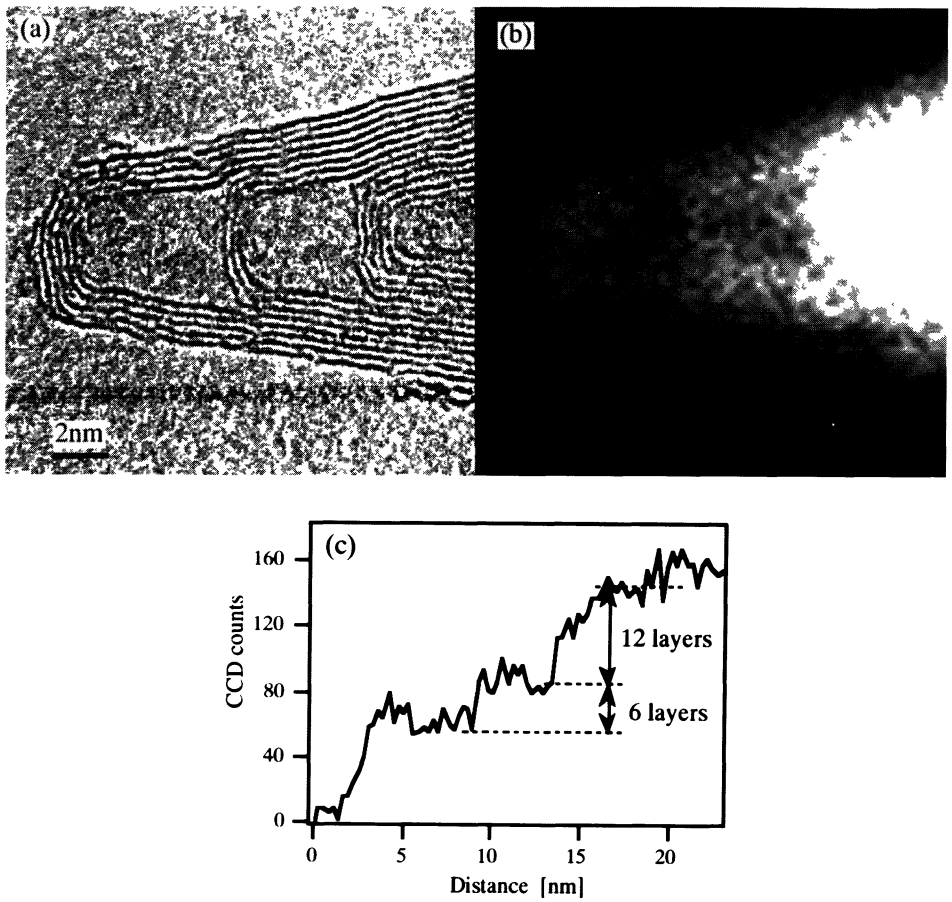

Fig. 6. — a) High-resolution lattice image of the conical tip region of nanotube and b) corresponding carbon distribution image. c) Stepwise intensity profile of the carbon distribution image along the cone axis of the nanotube tip.

case, however, the background intensity arising from the tail of valence electron excitations is small compared to the signal one ($I_i^b \ll I_i^s$), because the nanotubes are supported by themselves on a hole and composed of a small number of carbon atoms. Accordingly the SNR of the carbon distribution image of Figure 2b was proportional approximately to the square root of the signal intensity.

Figure 7 shows the SNR calculated for each binned pixel across the tube axis of the carbon image shown in Figure 2b. In the nanotube region the values of SNR are 5 to 9. If the value of SNR is equal to 3, the intensity of an elemental map corresponds to the minimum detectable number of atoms [13]. Since the observed SNR is larger than 3, it is sure that the carbon distribution image of Figure 2b is well discerned from the noise level. As mentioned in the intensity profiles of Figure 5, the minimum number of atoms detected in the carbon distribution image is 22 atoms per one binned pixel (0.28×0.28 nm^2). Consequently, the minimum detectable number of atoms per binned pixel should be less than 22 atoms under the present experimental conditions because the observed values of SNR are larger than the critical value of 3 that defines the detection limit.

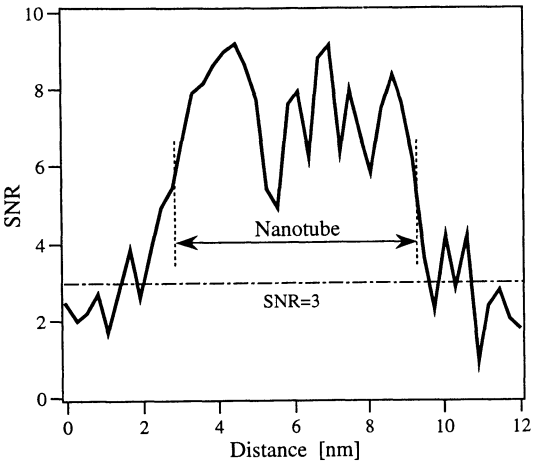

Fig. 7. — Line trace of signal-to-noise ratio (SNR) of the carbon distribution image of Figure 2b.

4. Conclusion

From the application of energy-filtering electron microscopy to the carbon nanotube the quantitative elemental imaging has been demonstrated, which is proposed for the useful method to determined the detection limit in imaging. The experimental intensity profile of the carbon image was in good agreement with the distribution of carbon atoms theoretically calculated from the structure of the nanotube. The difference of about 20 carbon atoms was clearly observed in the intensity profile at nanometer scale. From the SNR analysis of the carbon distribution image the detection limit was estimated to be less than 22 carbon atoms in one binned pixel ($0.28 \times 0.28\ nm^2$) under the present experimental conditions. For the ultimate single atom analysis [18] it should be necessary to irradiate with a much stronger electron beam than the present experiment. However, the nanotubes suffer structural distortion from intense electron irradiation, so that the detection limit actually evaluated is restricted by the stability of specimen to electron beam.

Acknowledgements

We would like to thank Mr. Y. Ohtuka of Toray corporation for providing the carbon nanotubes.

References

[1] Reimer L., in Advances in Electronics and Electron Physics, Vol. 81 (Academic Press, 1991) p. 43.
[2] Berger A., Mayer J. and Kohl H., *Ultramicrosc.* **55**(1994) 101.
[3] Berger A. and Kohl H., *Microsc. Microanal. Microstruct.* **3** (1992) 159.
[4] Berger A. and Kohl H., *Optik 92* (1993) 175.
[5] Iijima S., *Nature* **354** (1991) 56.
[6] Isoda S., Moriguchi S., Kurata H., Kobayashi T. and Uyeda N., *Ultramicrosc.* **39** (1991) 247.
[7] Krivanek O.L., Gubbens A.J., Dellby N. and Meyer C.E., *Microsc. Microanal. Microstruct.* **3** (1992) 187.

[8] Gubbens A.J. and Krivanek O.L., *Ultramicrosc.* **51** (1993) 146.

[9] Kurata H., Moriguchi S., Isoda S. and Kobayashi T., in Proc. of ICEM13, Paris, Vol. 1 (Les Editions de Physique, Les Ulis, 1994) p. 717.

[10] Mooney P.E., Bui D.N. and Krivanek O.L., in Proc. of ICEM13., Paris,Vol. 1 (Les Editions de Physique, Les Ulis, 1994) p. 213.

[11] Ajayan P.M., Colliex C., Bernier P. and Lambert J.M., *Microsc. Microanal. Microstruct.* **4** (1993) 501.

[12] Shuman H., Chang C.F. and Somlyo A.P., *Ultramicrosc.* **19** (1986) 121.

[13] Egerton R.F., Electron Energy-Loss Spectroscopy in the Electron Microscope (Plenum Press, New York and London, 1986).

[14] Ajayan P.M., Colliex C., Lambert J.M., Bernier P., Barbedette L., Tence M. and Stephan O., *Phys. Rev. Lett.* **72** (1994) 1722.

[15] Fano U., *Phys. Rev.* **102** (1956) 385.

[16] Pennycook S.J., *Contemp. Phys.* **23** (1982) 371.

[17] Browning N.D., Chisholm M.F. and Pennycook S.J., *Nature* **366** (1993) 143.

[18] Krivanek O.L., Mory C., Tence M. and Colliex C., *Microsc. Microanal. Microstruct.* **2** (1991) 257.